iScience

CellPress
OPEN ACCESS

Article

Cholesterol-induced suppression of Kir2 channels is mediated by decoupling at the inter-subunit interfaces

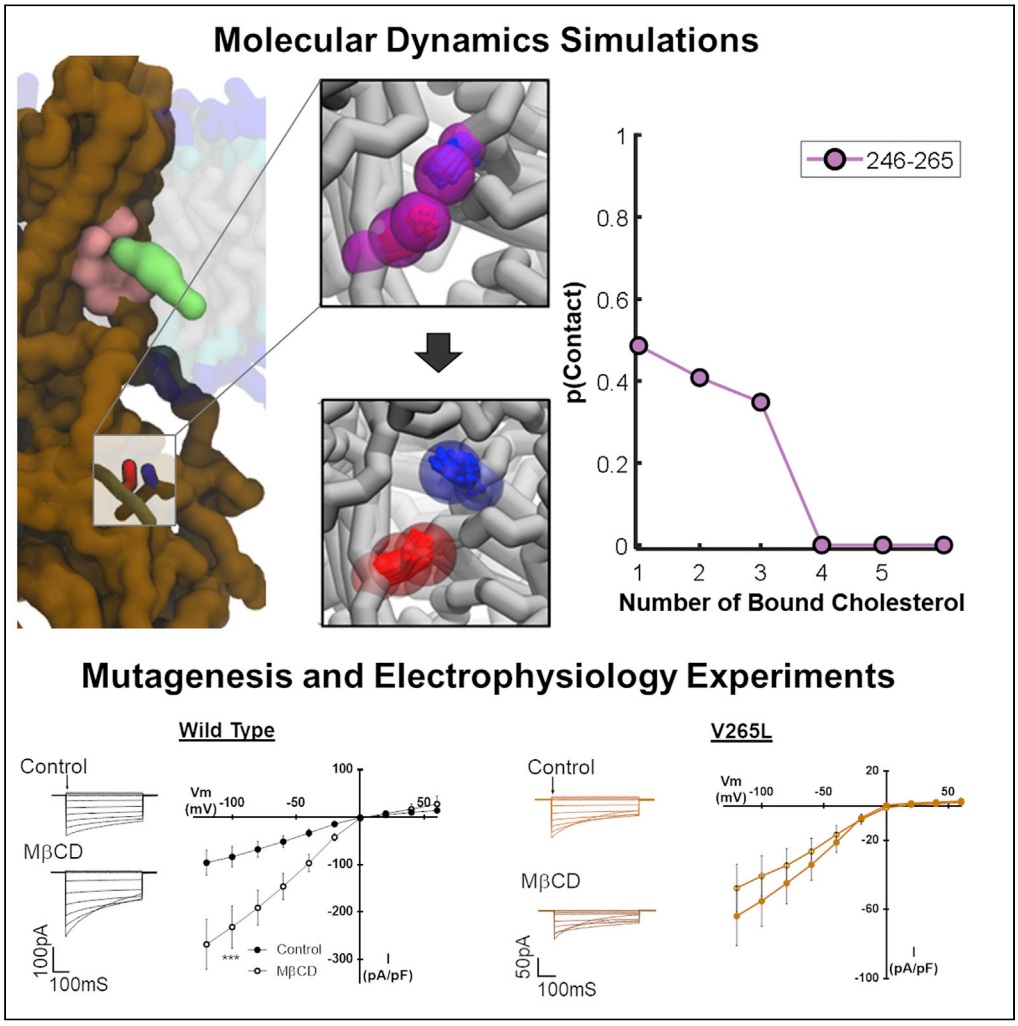

Nicolas Barbera, Sara T. Granados, Carlos Guillermo Vanoye, ..., Alfred L. George, Jr., Belinda S. Akpa, Irena Levitan

unz2ra@virginia.edu (N.B.)
akpabs@ornl.gov (B.S.A.)
levitan@uic.edu (I.L.)

Highlights

Coherent motion of Kir2.2 domains show subunit decoupling upon cholesterol binding

Cholesterol-induced decoupling correlates with the number of bound cholesterols

Point mutation of residues identified by network analysis abrogates the decoupling

Loss of decoupling results in loss or reversal of cholesterol sensitivity

Barbera et al., iScience 25, 104329
May 20, 2022
https://doi.org/10.1016/j.isci.2022.104329

iScience

CellPress
OPEN ACCESS

Article

Cholesterol-induced suppression of Kir2 channels is mediated by decoupling at the inter-subunit interfaces

Nicolas Barbera,[1,*] Sara T. Granados,[1] Carlos Guillermo Vanoye,[2] Tatiana V. Abramova,[2] Danielle Kulbak,[1] Sang Joon Ahn,[1] Alfred L. George, Jr.,[2] Belinda S. Akpa,[3,4,5,*] and Irena Levitan[1,6,*]

SUMMARY

Cholesterol is a major regulator of multiple types of ion channels. Although there is increasing information about cholesterol binding sites, the molecular mechanisms through which cholesterol binding alters channel function are virtually unknown. In this study, we used a combination of Martini coarse-grained simulations, a network theory-based analysis, and electrophysiology to determine the effect of cholesterol on the dynamic structure of the Kir2.2 channel. We found that increasing membrane cholesterol reduced the likelihood of contact between specific regions of the cytoplasmic and transmembrane domains of the channel, most prominently at the subunit-subunit interfaces of the cytosolic domains. This decrease in contact was mediated by pairwise interactions of specific residues and correlated to the stoichiometry of cholesterol binding events. The predictions of the model were tested by site-directed mutagenesis of two identified residues—V265 and H222—and high throughput electrophysiology.

INTRODUCTION

Many types of ion channels are suppressed by the elevation of membrane cholesterol in a variety of cell types (I. Levitan et al., 2010, 2014, 20). Originally, it was thought that these effects are because of changes in the physical properties of the bilayer, but analysis of sterol-channel interactions showed that this is not the case. Rather, previous experimental studies using chiral isomers indicated that cholesterol might mediate channel function through direct binding (Romanenko et al. 2002; Bukiya et al., 2011; Picazo-Juarez et al., 2011). Focusing on the family of the inwardly rectifying potassium channels (Kir) that are ubiquitously expressed in a variety of cells (Hibino et al., 2010), we previously found that although an increase in membrane cholesterol suppresses the currents (Romanenko et al. 2002; Romanenko et al., 2004), substituting cholesterol with its chiral analogue—epicholesterol—has the opposite effect, indicating that cholesterol-Kir interaction is stereospecific (Romanenko et al. 2002). We also demonstrated this cholesterol stereospecific effect and a lack of correlation with membrane fluidity for purified KirBac1 (D. K. Singh et al., 2009), a bacterial homologue of Kir. More recently, the stereospecificity of cholesterol-induced suppression of Kir2.1 was likewise demonstrated for purified Kir2.1 channels in liposomes (D'Avanzo et al., 2011). Furthermore, several other types of ion channels, including large-conductance Ca2+-sensitive K+ channels and Transient Potential Ca2+ channels, TRPV, have been shown to be regulated via direct stereospecific interactions (Levitan et al., 2014; Bukiya et al., 2011; Picazo-Juarez et al., 2011). We also showed that cholesterol binding is required for the suppression of Kir channels (D. K. Singh et al., 2011). Together, this evidence is indicative of direct binding being responsible for cholesterol regulation of ion channel function.

Previous studies identified several cholesterol-recognition motifs that helped establish some of the characteristics of cholesterol binding sites (Baier et al. 2011; Fantini and Barrantes 2013; Di Scala et al., 2017). However, these motifs appear to capture only a subset of the possible cholesterol binding sites (A. Rosenhouse-Dantsker 2017). Therefore, in our previous studies, we used multi-scale computational approaches, including docking analysis, atomistic, and coarse-grained molecular dynamics (MD) simulations and network analysis to provide unbiased insights into cholesterol binding to Kir2 channels (Avia Rosenhouse-Dantsker et al., 2013; Barbera et al., 2018). These studies led to the identification of specific cholesterol binding pockets within the transmembrane domains of Kir2.1 and Kir2.2 channel, where cholesterol dynamically explores its binding space (Avia Rosenhouse-Dantsker et al., 2013; Barbera et al., 2018).

[1]Division of Pulmonary and Critical Care Medicine, Department of Medicine, University of Illinois at Chicago, Chicago, IL 60611, USA

[2]Department of Pharmacology; Northwestern University Feinberg School of Medicine, Chicago, IL 60611, USA

[3]Division of Biosciences, Oak Ridge National Laboratory, Oak Ridge, TN 37830, USA

[4]Department of Chemical & Biomolecular Engineering, University of Tennessee, Knoxville, TN 37996, USA

[5]Molecular Biomedical Sciences, North Carolina State University, Raleigh, NC 27695, USA

[6]Lead contact

*Correspondence: unz2ra@virginia.edu (N.B.), akpabs@ornl.gov (B.S.A.), levitan@uic.edu (I.L.)

https://doi.org/10.1016/j.isci.2022.104329

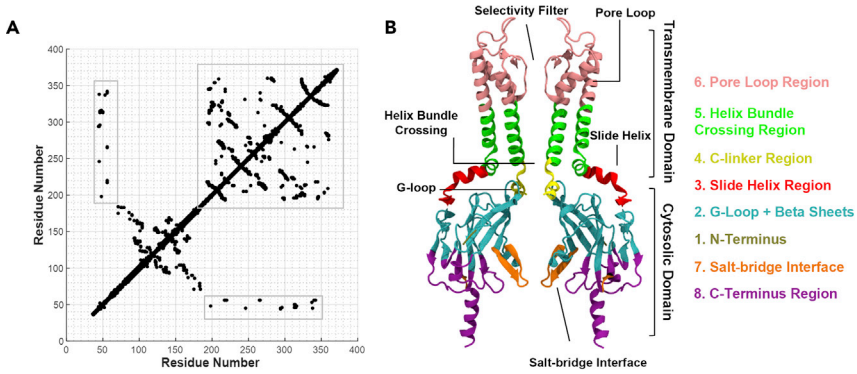

Figure 1. Identifying candidate regulatory domains on the Kir2.2 channel using a protein contact network

(A). A visualization of the consensus network is shown here as an adjacency matrix. Each dot represents a residue-residue interaction persistent for at least 90% of each respective simulation condition. Those dots on the diagonal correspond to the covalently bonded primary sequence of the protein, whereas dots off the diagonal correspond to non-covalent interactions between amino acids. The boxes denote the residue-residue interactions within the cytosolic domain of the channel.

(B). A visualization of the Kir2.2 channel, with the residues comprising each modularity group colored separately. Transmembrane and cytosolic domains are labeled along with functionally relevant regions of the channel. Domains are numbered according to the Kir2.2 primary sequence and arranged in the figure to match their location on the protein.

Although putative binding sites of cholesterol in Kir2.1/Kir2.2 channels have been identified, the mechanism by which cholesterol binding regulates channel activity is still poorly understood.

In this study, we use a combination of computational and experimental methods to investigate the effect of cholesterol on Kir2 channel mechanics, particularly on residue-residue interactions. Our computational studies show that increased levels of membrane cholesterol lead to a "decoupling" effect, whereby interactions between different domains of the channel are interrupted via the disruption of specific residue-residue interactions. This conclusion is tested further through *in silico* and *in vitro* mutagenesis of the residues identified in the decoupling between the domains, followed by high-throughput electrophysiology experiments.

RESULTS

In this study, our objective was to determine how cholesterol alters the dynamics of the Kir2.2 channel. As in our previous work (Barbera et al., 2018), we employed concepts from network theory to query the dynamic structure of the protein. Although we previously sought to identify sets of residues that concurrently contact a sterol ligand (i.e., a binding site), we now seek to identify groups of residues (candidate regulatory domains) whose motions relative to each other are altered by the presence of cholesterol. Using a network-based analysis, we (1) segregated the Kir2.2 protein structure into domains of coherent motion, (2) quantified how cholesterol changed interactions both between and within those domains, and (3) identified key residues that were implicated in these changes. We then used site-directed mutagenesis and electrophysiology to test the impact of these residues on cholesterol sensitivity of Kir2.2.

Identifying domains of coherent motion on the Kir2.2 channel

A network is a graphical representation of a complex system that displays agents of the system as nodes and interactions between them as edges. A protein contact network includes all amino acid residues of the protein as nodes and includes edges for those pairs of residues who maintain a proximity of less than 6 Å for at least 90% of an MD simulation's duration. To identify domains of coherent motion in the Kir channel, we first defined a protein contact network for each channel state (open and closed) and cholesterol concentration (15 mol % and 30 mol %). By preserving those edges that appeared in all conditions, we produced a consensus network reflecting those interactions that were conserved across all states and cholesterol conditions (Figure 1A). We then used a Louvain clustering algorithm to partition the network into eight modularity groups (Blondel et al., 2008). Upon mapping the modularity groups to the protein structure (Figure 1B), we observed that several groups map well to known functional domains of the channel. Other groups provide further insights into the structural dynamics of the protein. In particular, we note that the transmembrane helices of

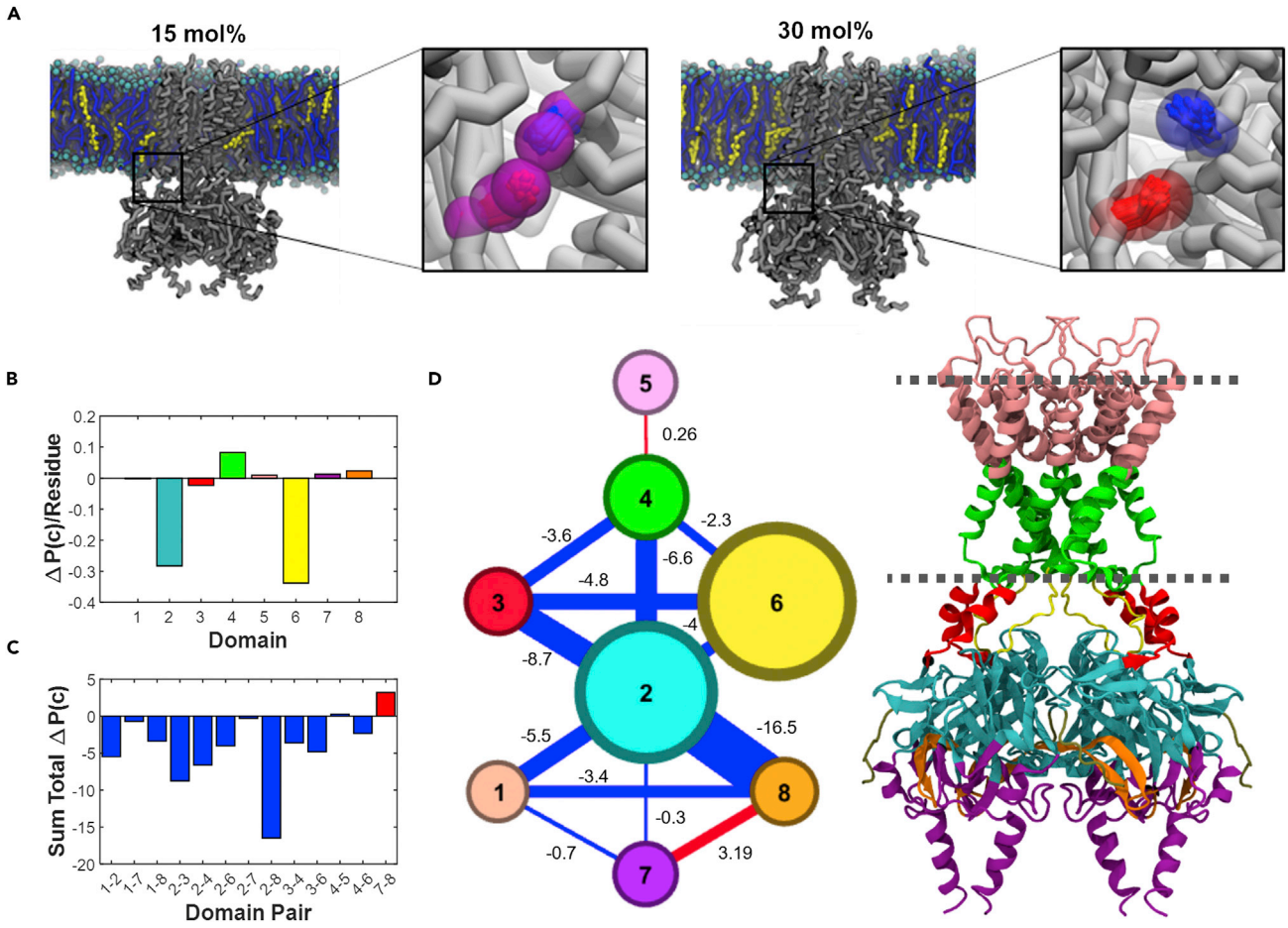

Figure 2. Uncovering cholesterol-mediated perturbation of candidate regulatory domains via Domain Difference Contact Networks

(A) Simulation snapshots of a residue interaction pair at two different membrane cholesterol concentrations, 15 mol % (left) and 30 mol % (right). Multiple snapshots are overlaid together to show the decoupling phenomenon. Van der Waal radii are shown as transparent spheres.

(B) The average change in contact probability per residue in each domain of the closed state channel. Individual bar plots are colored according to the schematic in Figure 1.

(C) Sum total change in contact probability between a pair of domains in the closed state of the channel. Bars are colored blue for negative values and red for positive ones.

(D) Visualization of the domain difference contact network along with the closed state of the channel as reference. Nodes are sized according to the magnitude of the corresponding bar in B. Edges connecting nodes are labeled, sized, and colored according to the bar plot in C.

the channel partitioned into two regions. The "inner" region (group 5) lies within the inner leaflet of the membrane, close to the membrane-cytosol interface and contains the helix bundle crossing. The "outer" region (group 4) is in the outer leaflet and includes the extracellular loop, the pore loop, and the selectivity filter. The slide helix (group 3), which was shown previously to be important for gating (Lee et al., 2016; Wang et al., 2016), partitioned into a separate modularity group. The cytosolic domain partitioned into 5 modularity groups that map to domains with known functional relevance. In particular: the c-linker group (group 6) acts in tandem with the slide helix to facilitate channel opening and closing, whereas the "salt bridge interface" group (group 8) has been shown to regulate channel sensitivity to its agonist, PIP2 (Borschel et al., 2017). The largest modularity group in the cytosolic domain is the "G-loop and beta sheet" region (group 2), which contains the G-loop, that works in tandem with the helix bundle crossing and the selectivity filter and the β-sheets forming the subunit-subunit interface (Wang et al., 2016; Borschel et al., 2017).

Cholesterol causes decoupling within specific dynamic domains in the Kir2.2 closed state

To determine how cholesterol perturbs motions within and between these candidate regulatory domains, we produced domain difference contact networks (DDCN, Figure 2). Each DDCN has nodes that represent

the previously identified candidate regulatory domains and edges that reflect contacts between the domains. By comparing the 15 mol % cholesterol and 30 mol % cholesterol simulations for a particular channel state (i.e., closed 30 mol % vs. closed 15 mol % or open 30 mol % vs. open 15 mol %), we calculated the net change in residue-residue contacts within a given domain ($DDCN_{XX}$) and sized the corresponding node accordingly. We then calculated the net change in residue-residue contacts between domains ($DDCN_{XY}$) and scaled the corresponding edge width accordingly. By using this analysis, we found that the most pronounced effect of an increase in membrane cholesterol is a decrease in net residue-residue contact probabilities – i.e., a "decoupling" effect. This decoupling is evident in the MD trajectory snapshot rendered in Figure 2A, which is representative of a residue-residue interaction that is perturbed in the presence of increased membrane cholesterol.

The decoupling phenomenon is most pronounced in the channel's closed state within two specific regions of the cytoplasmic domain (Figures 2B and 2D): (i) domain 2, which contains the G-loop, critical for channel gating(Pegan et al., 2005; Gupta et al., 2010) and (ii) domain 6, which contains the c-linker region, a sequence of residues that undergoes an order-disorder transition during channel opening(Clarke et al., 2010; Lacin et al., 2017). There is also a mild coupling effect observed in the transmembrane domain and little change in other domains. Here, in contrast, the only small changes in residue-residue interactions in both coupling and decoupling are observed in the open state of Kir2.2 upon increase in membrane cholesterol (Figure S1).

We also found that, upon an increase in membrane cholesterol, there is a net cumulative decoupling effect between Kir2.2 channel domains, and that effect is observed both in the closed (Figures 2C and 2D) and in the open configurations (Figures S1B and S1C). Specifically, for the closed state, we found large decreases between domains 2 (G-loop and beta sheet) and 3 (the slide helix) and domains 2 and 8 ("salt bridge interface"). Videos showing the motion of these domains can also be seen in Videos S1 and S2, which visualize a 15 μs MD trajectory at two different cholesterol concentrations. For the open state, the strongest net decoupling also involved domains 2 and 4, as well as domains one and 8 (outer region).

Decoupling phenomenon is dominated by a small subset of residue pairs

Our next objective was to identify specific residues that play key roles in the "decoupling" described previously. Focusing on the closed state of the channel, we examined the cholesterol-mediated change in contact probability for each pair of residues in the Kir channel (Figure 3A shows a dot plot where decreased contact probability is shown in blue and increased probability in red). Although, clearly, residue-residue contacts decreased for some pairs and increased for others (Figure 3A), a net change calculated for each residue (i.e., contact probability summed overall interaction partners), shows that the overall effect is clearly a decoupling (Figure 3B).

For those residues that experience decoupling, there is a wide range in the degree of the decoupling. To quantify this variability, we generated a histogram of all nonzero changes in pairwise contact probability and found that 90% of residue pairs experienced a change of less than 10% (Figure 3C). Furthermore, only 0.5% of contacts (38 pairs) were decoupled via a contact probability change of −33% or more. Interestingly, when these pairs are visualized on the protein structure (Figure 3D), we see that they are concentrated primarily within the cytosolic region of the channel, near the interface between individual subunits. This suggests that a small number of residue-residue pairs are playing a major role in the observed decoupling effect. The full list of these pairs is listed in Table S2.

The aforementioned analysis indicates that an increase in membrane cholesterol leads to a decoupling between specific Kir2.2 residues, but it does not discriminate between the possibilities that this effect is because of either a) changes in the membrane properties or b) specific cholesterol binding to the channel. To answer this, we looked at the subset of residues that showed the largest decrease in contact probability and inspected the magnitude of that change as a function of the number of cholesterol molecules bound to the Kir channel. Specifically, we identified 20 binding events as described previously (Barbera et al., 2018) and extracted the corresponding trajectory snapshots. The binding events occur at both 15 mol % and 30 mol % membrane cholesterol with the clear shift to higher occupancy at 30 mol % (Figure 3E). We then quantified the number of bound sterol molecules in each snapshot in both conditions and grouped the snapshots accordingly. Finally, for each group, we determined the average contact probability for the residue pairs indicated in Table S2. We found that there is a negative correlation between bound cholesterol at the previously determined putative sites and residue-residue contact probability for 10 pairs. That is, increasing numbers of

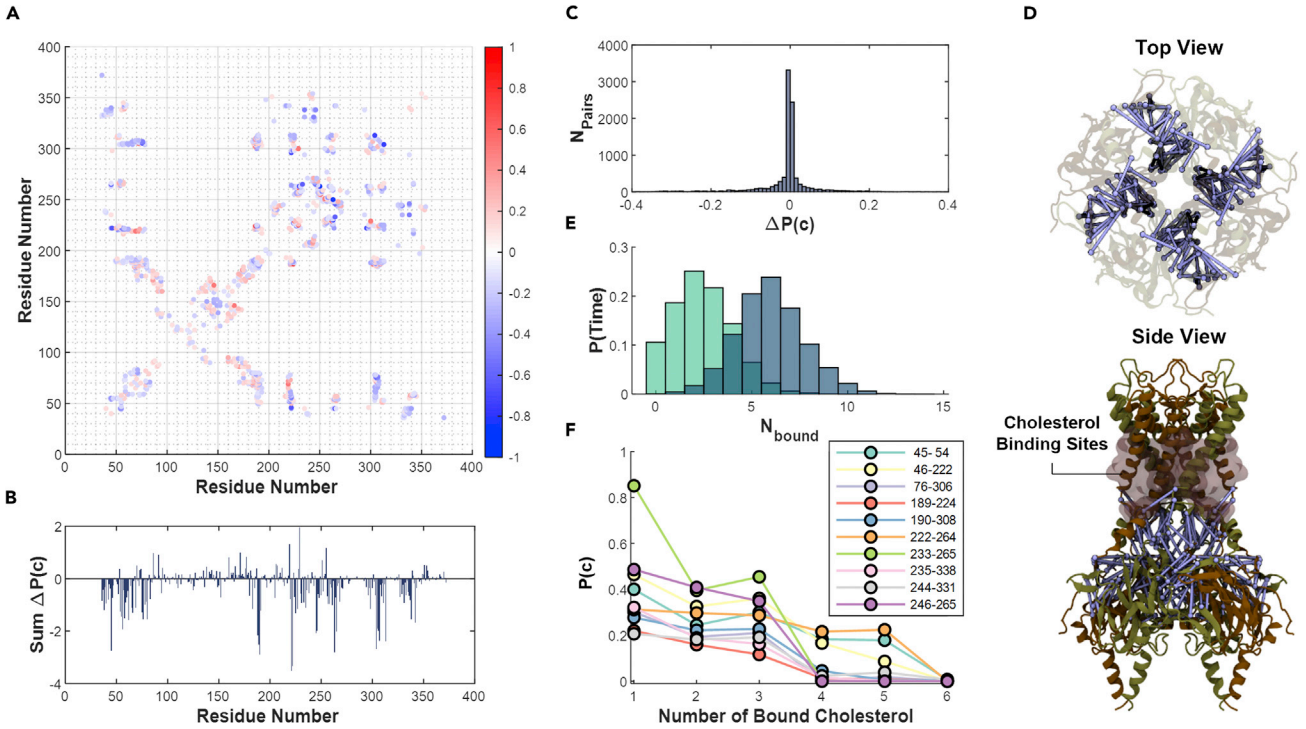

Figure 3. Specific residues mediate the domain decoupling phenomenon

(A) A difference contact network of the closed state of the channel, showing the change in contact probability of a pair of residues between the 15 mol % and 30 mol % membrane cholesterol conditions.

(B) The sum total change in contact probability of every residue in Kir2.2 between the 15 mol % and 30 mol % membrane cholesterol conditions.

(C) A histogram of all nonzero changes in contact probabilities for residue pairs in the closed state.

(D) Visualization of the 38 residue pairs with a greater than 35% decrease in contact probability. Pairs are visualized blue bonds connecting the alpha carbons of each residue. The previously identified cholesterol binding sites are visualized as a pink transparent surface for reference. Individual subunits are colored brown and tan.

(E) Histogram of the number of cholesterol bound to previously identified binding sites over the simulations in the 15 mol % condition (green) and 30 mol % condition (blue).

(F) Average residue-residue contact probability for a given pair when 1 to 6 cholesterol are bound to the binding sites of the closed state of the channel.

bound cholesterol in the transmembrane domain leads to decreased contact probability for residue pairs in the cytosolic domain (Figure 3F) – irrespective of the bulk cholesterol content of the membrane. Indeed, at the highest cholesterol occupancy, these residue pairs eventually became completely decoupled (p_{ij}~0).

Recently, it was shown that cholesterol forms dimers in the lipid membrane and that these dimers play a role in stabilizing the inactivated state of the bacterial Kir channel (Elkins et al., 2021; Borcik et al., 2022). Therefore, we investigated here whether the binding events that lead to residue decoupling were the result of single cholesterol molecules or cholesterol dimers. For each of the cholesterol binding events at both membrane cholesterol concentrations, we quantified the presence or absence of additional cholesterol molecules within 6 angstrom of the binding cholesterol molecules over the course of the simulations. We then compared this to the time course data of the cholesterol-channel interactions for each binding event (Figure S2). For each binding event, we calculated a phi coefficient quantifying the correlation between a cholesterol-channel interaction and a cholesterol-cholesterol interaction (Figure S3). We found that cholesterol-channel and cholesterol-cholesterol interactions appeared to be anticorrelated. That is, rather than forming dimers, cholesterol binds to the non-annular binding sites as individual molecules.

Site-directed mutagenesis to test decoupling predictions

In silico

To test whether the decoupling described previously is implicated in cholesterol sensitivity, we first performed simulations with point mutations of residues that were identified in the previous analysis and

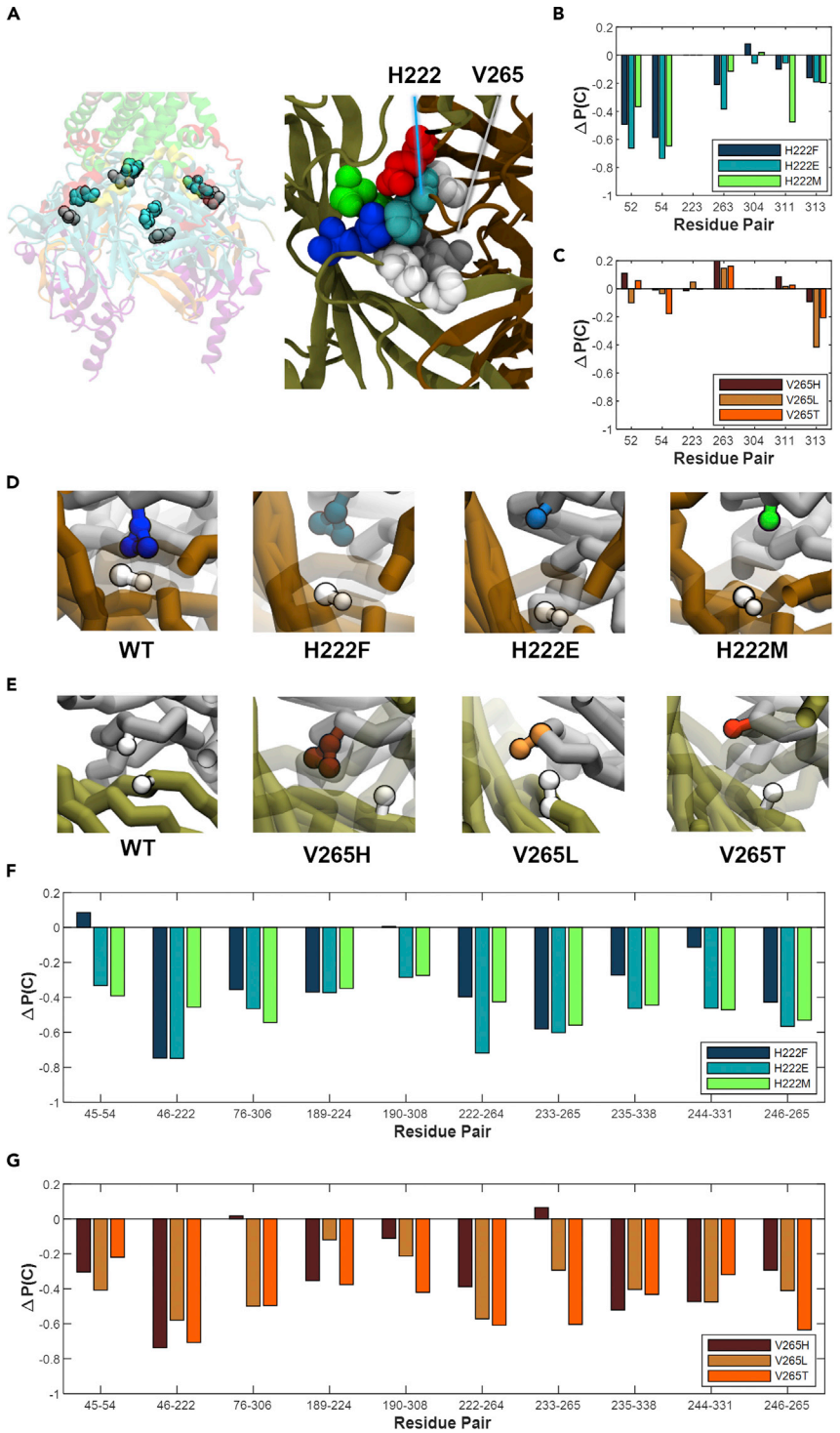

Figure 4. Mutations to residues H222 and V265 alter the interaction environment of the channel

(A). Visualization of residues H222 (Cyan) and V265 (Gray) (left), along with surrounding residues (right). Surrounding residues are colored by polarity: red is negatively charged, blue is positively charged, green is polar, and white is nonpolar. Individual subunits are colored tan and brown, respectively.

(B). Change in pairwise contact probability between residue 222 and each of the residues in A in the wild type versus mutant channel simulations at 15 mol % cholesterol.

Figure 4. *Continued*
(C). Change in pairwise contact probability between residue 265 and each of the residues in A in the wild type versus mutant channel simulations at 15 mol % cholesterol.
(D). Snapshots of residue pair Val46-His222 in the 15 mol % cholesterol condition for the wild type and mutated His222 systems.
(E). Snapshots of residue pair Leu246-Val265 in the 15 mol % cholesterol condition for the wild type and mutated V265 conditions.
(F). Change in pairwise contact probability between the wild type and His222 mutant channels for the residue pairs from Figure 3F. Contact probabilities are calculated from the 15 mol % cholesterol condition.
(G). Change in pairwise contact probability between the wild type and V265 mutant channels for the residue pairs from Figure 3F. Contact probabilities are calculated from the 15 mol % cholesterol condition.

then determined whether these substitutions alter the decoupling phenomenon. We chose to mutate residues that met the following criteria: 1) located within the cytosolic region of the channel (specifically, group 2) and near the interface of two subunits, 2) exhibit decreased contact probability of greater than 35% because of increased cholesterol, and 3) experience a decoupling effect that depends on number of bound cholesterol. Given these criteria, we identified two residues, H222 and V265. These residues are shown in Figure 4A, along with their surrounding residues. As can be seen in the image, the environment surrounding H222 and V265 consists of polar, nonpolar, and positively-charged and negatively-charged residues. Consequently, both residues were mutated with substitutions that test the effect of different physicochemical properties on the residue's interactions. Specifically, H222, a positively charged residue was mutated to: a nonpolar residue (H222M), a negatively charged residue (H222E), and a nonpolar residue possessing an aromatic ring (H222F). Likewise, for V265, a nonpolar, non-charged residue was mutated to a nonpolar residue of larger size (V265L), a positively charged residue (V265H), and a polar non-charged residue (V265T). The two key residues and the surrounding environment for each of their mutations are shown in Figure S4.

To explore the impact of these mutations on the channel dynamic behavior, we ran simulations of each of the six mutant channels at both 15 and 30 mol % cholesterol, similar to simulations of the WT channel. Each simulation condition was run for 5 μs with 5 replicates, totaling 25 μs per condition. For each mutation, the closed state of the channel was used as the reference to generate the structure. This was done for two reasons. First, because the elastic network used in the Martini coarse-grained model constrains the conformation of the channel to a single state, we chose to run the mutant channel simulations in the conformation where the effects on the aforementioned residues were observed – namely, the closed channel. Second, we chose to focus on closed state simulations because previous studies of channel kinetics suggested that cholesterol stabilizes Kir2 channels in the closed state (Romanenko et al. 2002; 2004).

First, we explored the impact of each of these mutations on the immediate environment of the mutated residues by calculating the shifts in the contact probabilities between the mutated residues and six neighboring residues as compared to the WT. This analysis showed that substituting H222 with the residues defined previously resulted in a decoupling of the mutated residue from its environment (Figure 4B), whereas substituting V265 with the residues defined before had a more subtle and heterogeneous effect, where some residue pairs showed decreased coupling, whereas others showed increased coupling (Figure 4C). Next, we looked at the impact of all of these mutations on the contact probabilities of the residue pairs identified in Table S2 and Figure 3F, i.e., those residue pairs which were decoupled by an increase in membrane cholesterol and predicted to be critical for cholesterol sensitivity of the channels. We found that all six mutations lead to decoupling of the residue pairs. Snapshots of this decoupling phenomenon are shown in Figure 4D and 4E. An example of this decoupling (H222E, residues 46 and 222) is also shown in Videos S3 and S4. When quantified, the effect of each mutation on these residue pairs shows a near universal and profound decoupling effect (Figures 4F and 4G).

To determine the impact of these mutations on cholesterol-induced changes in the dynamics of the channel, we repeated our PCN-based analysis of the changes in interactions *between* and *within* the structural domains for each mutant channel between the low and the high levels of cholesterol. We found that for all mutants, the cholesterol-dependent decoupling effect seen in the WT channel mostly disappears or is even reversed. The changes in interactions between and within domains were smaller when compared to the WT channel (Figure 5). In particular, we no longer observed the large decoupling effects seen within groups 2 and 6 for the WT channel. Likewise, the magnitude of the change in interactions between groups was much

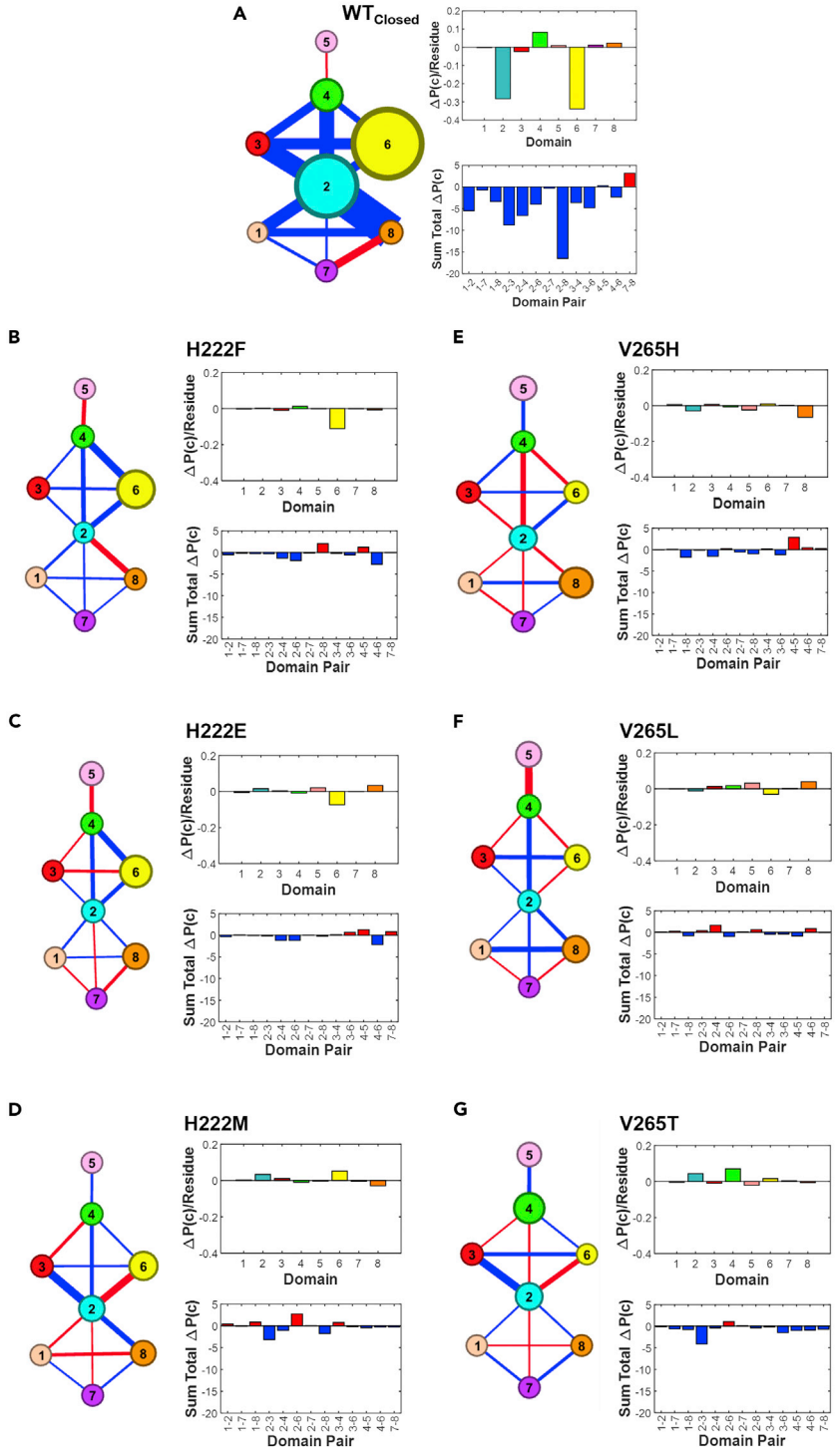

Figure 5. *In silico* Mutations alter inter-domain and intra-domain interactions

(A). Visualization of the domain difference contact network for the closed state of the WT channel. The size of the nodes and edges are scaled according to the adjacent bar plots: (Right, top) Bar plot of the change in contact probability per residue within each domain. (Right, bottom) sum total change in contact probability between domains. The DDCN and bar plots are reproduced from Figure 2 for comparison.

Figure 5. *Continued*
(B–G). Visualizations of the domain difference contact networks generated from the simulations of the mutant channels. Each network corresponds to the labeled mutation. Nodes and edges are scaled according to the adjacent bar plots for each mutant. Note that the y axes of the mutant channel bar plots are scaled to match A for comparison. Mutations are: H222F (B), H222E (C), H222M (G), V265H (E), V265L (F), and V265T (G).

lower than the observed changes in the WT channel. These observations provided us with a strong tool to test whether cholesterol-induced decoupling phenomenon affects cholesterol sensitivity of Kir2.2. Specifically, given that these mutations abrogated the cholesterol-mediated decoupling effect *in silico*, we hypothesized that changing these residues will alter Kir2.2 sensitivity to cholesterol *in vitro*. We tested this hypothesis using site-directed mutagenesis and electrophysiological recordings, as described in the following section.

Electrophysiology

To test the predictions of the model experimentally, we generated the six single-point mutations that we have verified to impact cholesterol-induced decoupling in the MD simulations. As described earlier, three substitutions were performed for V265: Kir2.2^{V265L}, Kir2.2^{V265H}, and Kir2.2^{V265T} and three for H222: Kir2.2^{H222F}, Kir2.2^{H222M}, and Kir2.2^{H222E}. Functional sensitivity of these Kir2.2 mutants to cholesterol, as compared to WT Kir2.2, was tested by expressing the channel proteins in CHO cells. The mutants were generated in a Kir2.2-GFP fusion protein to verify mutant expression and co-localization with the membrane using a combination of flow cytometry and fluorescence microscopy. Typical images shown in Figure S5A demonstrate that both Kir2.2 WT and all Kir2.2 mutants generated in this study localize primarily in the plasma membrane as indicated by their co-localization with the membrane marker, WGA. In addition, the expression of Kir2.2 and its mutants was quantified by flow cytometry showing no significant differences in the number of cells successfully transfected or in the mean fluorescence intensity indicating that neither of the mutations significantly affected Kir2.2 expression or membrane localization (Figure S5B).

Whole-cell currents were recorded using high-throughput automated patch clamps that allow us to simultaneously record multiple cells expressing WT or mutant channels (Vanoye et al., 2018). Cholesterol sensitivity was tested by depleting cellular cholesterol using MβCD before the recording as previously described (Romanenko et al. 2002; 2004). To exclude the contamination of nonspecific currents, recordings were performed in the absence and presence of Ba^{2+}, a blocker of Kir channels (Vanoye and Reuss 1999; Kubo et al., 2005). Cholesterol depletion was verified using Amplex-red kit (Figure S6).

In each experiment, we evaluated cholesterol sensitivity of all three mutants of either V265 or H222 along with WT Kir2.2 channels included as control (between 29 and 59 cells were recorded for each condition). Wild-type Kir2.2 currents showed typical biophysical properties of Kir, the inward rectification and time-dependent inactivation (see traces in Figures 6A and 6F). As expected, WT channels responded to cholesterol depletion with a significant (two to three-fold) increase in K^+ current density (Figures 6A and 6F). However, no cholesterol sensitivity was observed when V265 was mutated to histidine or leucine or when H222 was substituted with phenylalanine or glutamic acid. Notably, despite the loss of cholesterol sensitivity of these mutants, the current densities generated by the mutated channels were not larger than the WT Kir2.2—as could be expected—because they are not suppressed by membrane cholesterol. Instead, the currents generated by most of the mutated channels are significantly smaller than those generated by WT Kir2.2 in the same experiment. This decrease in current density is not because of decreased expression, as shown in the Figure S5, but should be attributed to the complex effects of single mutations on the channel function, which is discussed in more detail in the discussion section. Moreover, Kir2.2^{V265T} showed a reversal of cholesterol sensitivity with cholesterol depletion decreasing current density rather than increasing it. A similar but smaller reversal was observed for Kir2.2^{H222M}. Most importantly, all six mutations had profound effects on cholesterol sensitivity, providing strong evidence for the central roles of these residues in cholesterol sensitivity of Kir2.2 channels and validating the predictions of our model.

DISCUSSION

Cholesterol regulation of membrane proteins—ion channels in particular—has been a focus of numerous studies, but the mechanistic basis of the functional effect remains poorly defined. In this study, focusing on Kir2.2 channels, we provide evidence for the concept that cholesterol sensitivity of an ion channel can result from the decoupling between channel functional domains – a phenomenon induced by cholesterol binding

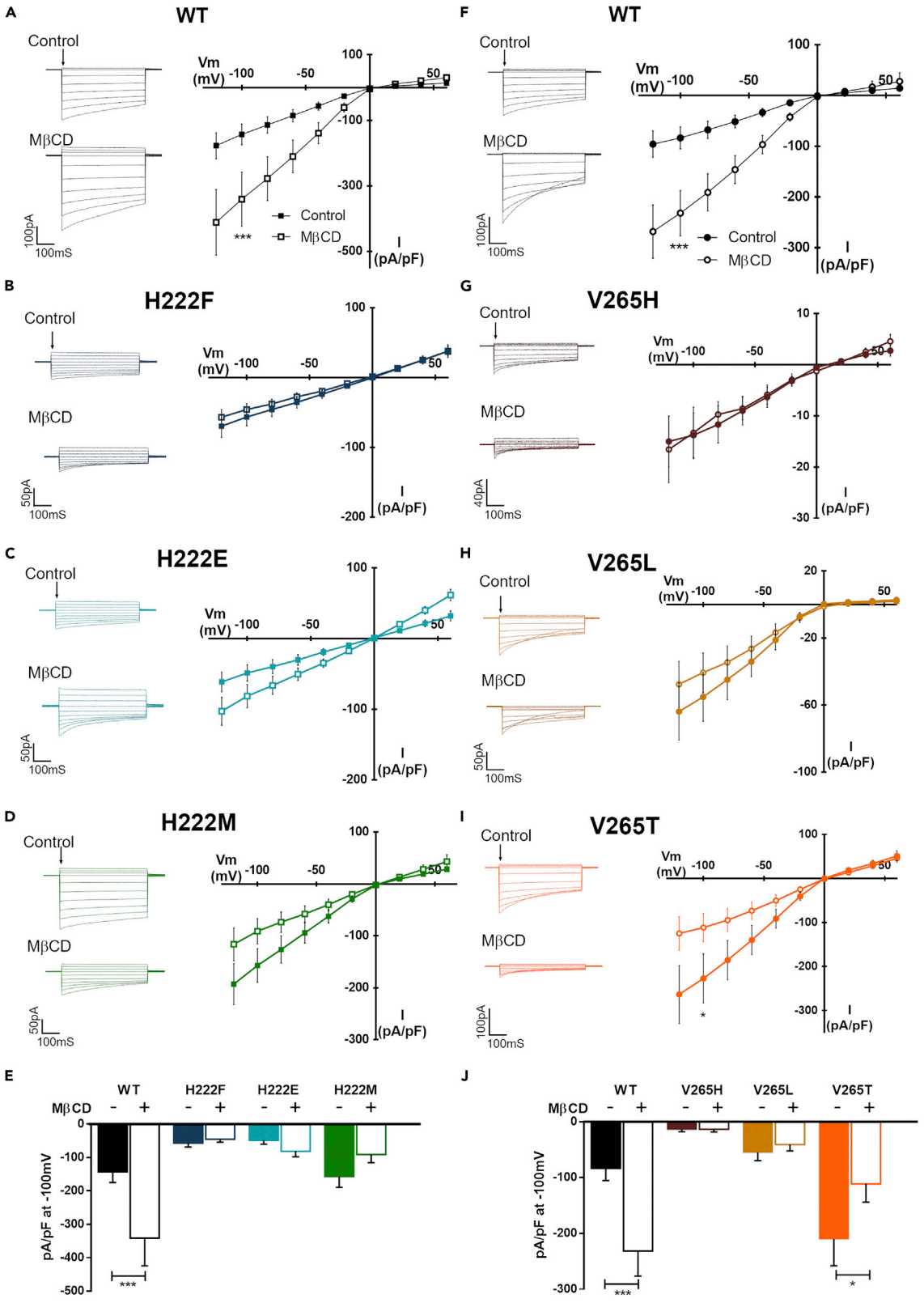
A
WT
Control
MβCD
100pA
100mS
Vm (mV)
-100
-50
50
100
-100
-300
-500
Control
MβCD
***
I (pA/pF)
F
WT
Control
MβCD
100pA
100mS
Vm (mV)
-100
-50
50
100
-100
-200
-300
Control
MβCD
***
I (pA/pF)
B
H222F
Control
MβCD
50pA
100mS
Vm (mV)
-100
-50
50
100
-100
-200
I (pA/pF)
G
V265H
Control
MβCD
40pA
100mS
Vm (mV)
-100
-50
50
10
-10
-20
-30
I (pA/pF)
C
H222E
Control
MβCD
50pA
100mS
Vm (mV)
-100
-50
50
100
-100
-200
I (pA/pF)
H
V265L
Control
MβCD
50pA
100mS
Vm (mV)
-100
-50
50
20
-20
-60
-100
I (pA/pF)
D
H222M
Control
MβCD
50pA
100mS
Vm (mV)
-100
-50
50
100
-100
-200
-300
I (pA/pF)
I
V265T
Control
MβCD
100pA
100mS
Vm (mV)
-100
-50
50
100
-100
-200
-300
*
I (pA/pF)
E
WT
H222F
H222E
H222M
MβCD
-
+
-
+
-
+
-
+
0
-100
-200
-300
-400
-500
pA/pF at -100mV
***
J
WT
V265H
V265L
V265T
MβCD
-
+
-
+
-
+
-
+
0
-100
-200
-300
pA/pF at -100mV
***
*

Figure 6. Functional response of Kir 2.2 mutants to cholesterol

Representative traces (left) and current vs. voltage relationships (I/V) (right) for Kir 2.2 WT (A) as reference for V265 mutations: Kir 2.2^{V265H} (B), Kir 2.2^{V265L} (C), and Kir 2.2^{V265T} (D). E. Current density at −100mV for Kir 2.2^{V265} mutants from the I/V curves represented on A-D. Representative traces and I/V curves for Kir 2.2 WT (F) as reference for H222 mutations: Kir 2.2^{H222F} (G), Kir 2.2^{H222E} (H), and Kir 2.2^{H222M} (I). J. Current density at −100mV for Kir 2.2^{H222} mutants from the I/V curves represented on F-I. Filled symbols and bars indicate control cells, whereas empty symbols and bars denote cells treated with MβCD 2.5 mM for 45 min. Arrows on the traces show the time point (10ms) when the I/Vs were measured. All data are represented as mean ± SEM $p \leq 0.001$:***, $p \leq 0.05$:*.

to non-annular sites within the channel protein. Notably, this decoupling does not occur at the cholesterol binding sites but instead occurs remotely at inter-subunit interfaces within the cytosolic domain. This conclusion is based on a combination of coarse-grained molecular dynamics simulations of Kir2.2 in membranes with varying levels of cholesterol and a protein contact network-based analysis to interrogate the effects of membrane cholesterol on the dynamic structure of Kir2.2. The analysis was further validated by testing the effects of point mutations both *in silico* and electrophysiologically. In particular, we identified clusters of residues in the channel that formed domains of coherent movement, which corresponded to previously identified structures of functional relevance in the channel, and found that a higher level of membrane cholesterol reduced the likelihood of residue-residue contact within two specific cytoplasmic domains. Furthermore, single-point mutations of those residues identified as playing a key role in the decoupling effect resulted in the abrogation of this cholesterol-induced decoupling effect and abrogation or even reversal of cholesterol-induced suppression of Kir2.2 function.

Earlier studies proposed membrane deformation energy, membrane stress, and hydrophobic mismatch between the channel and the lipid bilayer as the mechanisms for cholesterol-induced suppression of ion channel function (Chang et al., 1995; Lundbaek et al., 1996). However, an increasing number of studies show that cholesterol regulates ion channels by direct binding – shifting the attention to identifying cholesterol binding sites (Levitan et al., 2014). Today, cholesterol binding sites have been identified in several types of ion channels: Kir2.½.2 (Avia Rosenhouse-Dantsker et al., 2013; Barbera et al., 2018; Fürst et al., 2014), TRPV1 (Picazo-Juarez et al., 2011), BK (A. K. Singh et al., 2012), nAChR (Brannigan et al., 2008; Fantini and Barrantes 2013), and GABA1 (Henin et al., 2014). In most cases, the binding sites were identified at non-annular hydrophobic pockets rather than on the membrane-protein interface. Recently, we showed that the direct interactions between cholesterol and Kir2.2 are complex and multifaceted, with multiple short-lived and long-lived interactions occurring simultaneously on the membrane-protein interface and at non-annular pockets, respectively (Barbera et al., 2018). Single channel kinetics of Kir2.1 channels suggested that cholesterol stabilizes Kir2 channels in the closed state and creates a population of "silent channels" (Romanenko et al. 2002; 2004). We also identified multiple residues outside of cholesterol binding sites that are important for cholesterol sensitivity of Kir2 channels, particularly in the cytosolic domain: the "belt" of residues near the interface with the transmembrane domain (Epshtein et al., 2009; Avia Rosenhouse-Dantsker et al., 2011), and the cytosolic gating machinery situated around the G-loop, which controls pore opening (A. Rosenhouse-Dantsker and Levitan 2012). There is also a significant overlap between the residues involved in the sensitivity of Kir2 channels to cholesterol and to regulatory phospholipid PIP2 (Epshtein et al., 2009; Avia Rosenhouse-Dantsker et al., 2014) essential for Kir function (Hibino et al., 2010), and cholesterol depletion strengthens the interaction of Kir2.1 channels with PIP2 (Avia Rosenhouse-Dantsker et al., 2014, 2). Interestingly, in GIRK channels that are facilitated rather than suppressed by cholesterol (A. Rosenhouse-Dantsker and Levitan 2012), cholesterol binding was shown recently to stabilize their interaction with PIP2 (Mathiharan et al., 2021). Cholesterol binding was also shown to stabilize the conformational dynamics of a GPCR receptor, serotonin1A (Kumar et al., 2021). Overall, however, little is known about the link between cholesterol binding and functional regulation of ion channels and receptors. In this study, we provide evidence for a mechanism for cholesterol-induced regulation of ion channels via decoupling between the channel domains of coherent motion.

In this study, we addressed the mechanism of cholesterol-induced suppression of Kir2 channels by using protein contact networks derived from pairwise residue interactions. Protein contact networks have been used to study allosteric pathways in proteins and the effects of ligand binding (Daily and Gray 2009; Dokholyan 2016). By adopting a protein contact network analysis based on the consensus network approach from Yao et al. (Yao et al. 2018), we interrogated the effects of changing membrane cholesterol on the dynamics of different structural domains in the channel. The simulations were designed to mimic the changes in cholesterol that occur in mammalian cells under typical experimental conditions used to test the sensitivity of the channels to cholesterol. Multiple studies showed that the typical level of plasma cholesterol is ~30 mol % (Meer et al., 2008; Ingólfsson et al., 2014) and that exposure to methyl-β-cyclodextrin

(MβCD), the most commonly used method to test cholesterol sensitivity of membrane proteins, results in partial removal of cholesterol from the membrane (Zidovetzki and Levitan 2007). Earlier studies from our lab (Romanenko et al., 2004; 2002) as well as the current study (Figure 5), demonstrated that a ~2-fold decrease in membrane cholesterol results in a pronounced increase in the activity of Kir2 channels. A stronger cholesterol removal is not desirable because it results in cell toxicity and nonspecific effects on membrane proteins. Thus, we focused on comparing two physiologically relevant cholesterol levels, 15 mol % and 30 mol %, a difference that we know results in a significant decrease in Kir2 activity. We found that the primary effect of increasing membrane cholesterol was "decoupling," a decrease in net contact probability for residue pairs both within and between domains. Moreover, we also identified the specific residues that mediate these interactions. The location of these residues provided further insights into the nature of cholesterol-induced decoupling. The residue pairs that experienced large changes in contact probability are located in the cytosolic domain of Kir2.2, distant from the previously identified cholesterol binding sites (Avia Rosenhouse-Dantsker et al., 2013; Barbera et al., 2018; Fürst et al., 2014). Furthermore, these residues appeared predominantly in two specific domains defined by our network analysis: group 6 containing the C-linker and group 2 containing the G-loop region, which are both known to be involved in the gating machinery of Kir2.2 (Pegan et al., 2005; Gupta et al., 2010; Clarke et al., 2010; Lacin et al., 2017). The decoupling effect is most pronounced at the interface between channel subunits. This is notable because interactions at the subunit interface stabilize Kir2 channels in the closed state (Wang et al., 2016; Borschel et al., 2017).

Having found cholesterol-mediated decoupling effects, we then hypothesized that the changes in coupling within domains might reflect a) strong contributions of a small set of residues and/or b) more subtle contributions from a large number of residues. Further analysis showed that a large part of the decoupling effect was mediated by a small number of residues that experience large (>33%) decreases in contact probability as membrane cholesterol increases. These results suggested that the domain-level effects were influenced by a small set of pairwise interactions, concentrated predominantly in the cytosolic region of the channel and distinct from the previously identified cholesterol binding sites. Most interestingly, we found that the contact probability between these residues negatively correlates with the stoichiometry of cholesterol binding to those sites.

Our analyses of single-point mutations, both *in silico* and by electrophysiology, support the idea that individual residues make large contributions to the decoupling phenomenon. *In silico* analysis demonstrated that single-point mutations of V265 and H222 resulted in the loss of cholesterol-dependent decoupling not only within the specific domains of these residues but also globally between the domains of the channels. Besides, electrophysiological studies showed that all of these mutations led to the abrogation or even reversal of the cholesterol effects. As pointed out earlier, the loss of cholesterol sensitivity of Kir2.2 mutants did not correlate with an increase in the current density generated by the mutated channel. This is consistent with our previous studies showing no clear correlation between the sensitivity of Kir2.1 channel mutants to cholesterol and their current density under control conditions (Epshtein et al., 2009; Avia Rosenhouse-Dantsker et al., 2013; Ahn et al., 2022). The phenomenon should instead be attributed to the complex effects of single point mutations on the channel structure, possibly including long-distance effects (A. Rosenhouse-Dantsker and Levitan 2012). On a more conceptual level, mutations may shift the conformation state of a channel in such a way that it makes it more difficult for the channel to transit from the closed to open states regardless of the sensitivity of the channels to cholesterol. It is also noteworthy that none of the mutations generated in this study affected the expression or membrane localization of Kir2.2 channels, suggesting that the loss of cholesterol sensitivity of the mutant channels is not related to changes in the channel expression levels.

Mechanistically, these alterations in inter-subunit coupling may be the result of local changes in the arrangement of residues surrounding V265 and H222, with specific mutations facilitating the strengthening of the couplings. Specifically, H222 is surrounded by polar and charged residues; therefore, mutations that affect polarity and size, such as Kir2.2^{H222M}, may reduce steric clashing and cause the oppositely charged residues E304 and R313 from different subunits to couple more effectively. Besides, V265, which is surrounded by predominantly nonpolar residues, alterations to the polarity of the residue, such as with V265T and V265H, may shift it away from the surrounding nonpolar residues, altering the inter-subunit interface. It is also an intriguing possibility that single-point mutations on the inter-subunit interface may have secondary distant effects on the interaction of the channels with PIP2, which we showed to be strengthened by cholesterol depletion (Avia Rosenhouse-Dantsker et al., 2014). If the current mutations

abrogate the strengthening of PIP2-Kir2.2 interaction, it might contribute to the loss of cholesterol sensitivity of the channels, and this possibility will be explored in our future studies.

Recent studies have shown that cholesterol forms dimers in the lipid membrane and that these dimers help to stabilize the inactivated state of the bacterial Kir channel. Therefore, we investigated whether the identified binding events facilitating the decoupling phenomenon were the result of cholesterol dimers. Although it is possible that cholesterol dimers form in the lipid bilayer, the evidence from our simulations suggests that these events do not correlate with the binding events identified in the current study. One reason for this difference could be the difference in channels studied. It has been well established that different families of Kir channels are regulated differently by cholesterol (Zakany et al., 2020), which may affect the formation of dimers in the binding site.

In conclusion, we performed a combination of coarse-grained molecular dynamics simulations, site-directed mutagenesis, and electrophysiology experiments to elucidate the effects of cholesterol binding on the structural dynamics of the channel. Using a network theory-based approach, we found that increased membrane cholesterol causes a "decoupling" effect between specific domains within the channel and that this effect is mediated by a small number of residue-residue interaction pairs that are predominantly located at the interface between channel subunits. A decoupling within domains of coherent motion provides a mechanism of cholesterol regulation of ion channels.

Limitations of the study

In interpreting the results of our coarse-grained simulations, there are limitations to consider which have been outlined in a number of reviews (J. Marrink et al., 2013; Grouleff et al., 2015; Hedger and Sansom 2016). The Martini model encompasses a 4-to-1 mapping of heavy atoms into coarse grained particles of specific physicochemical properties. This mapping allows for longer simulation times at the price of atomic resolution and smoothened energy landscapes (Alessandri et al., 2019). In addition, Martini coarse-grained simulations of proteins require an elastic network to stabilize the secondary and tertiary structures of the protein. This restricted our individual simulations to a single conformational state. However, even with the limitations imposed by coarse graining, the trade-off in simulation length allowed us to observe dynamics on timescales not easily accessible by atomistic simulations, but which have been shown to be important for cholesterol binding (Barbera et al., 2018). The nature of cholesterol binding to the channels with multiple hydrophobic interactions and with the cholesterol molecule dynamically exploring its binding pockets with multiple poses (Avia Rosenhouse-Dantsker et al., 2013; Barbera et al., 2018) also makes it difficult to identify possible mutations that may result in the loss of cholesterol binding, which could be an elegant way to further validate our conclusions. Although it is unlikely that a single-point mutation in the binding site would prevent cholesterol binding in one of the alternative poses, identifying a set of mutations required to achieve this would be interesting and valuable and should be pursued in the future. It would also be interesting to investigate how changes in PIP2 distribution that occur in response to cholesterol depletion affect cholesterol sensitivity of Kir2.2 and its mutants. We have shown previously that cholesterol depletion facilitates the interaction of Kir2.1 channels with PIP2 (Epshtein et al., 2009; Avia Rosenhouse-Dantsker et al., 2014), which might contribute to the increase in channel activity. It is an intriguing possibility that single-point mutations on the inter-subunit interface may have secondary distant effects on the interaction of the channels with PIP2, and it will be explored in our future studies.

STAR★METHODS

Detailed methods are provided in the online version of this paper and include the following:

- KEY RESOURCES TABLE
- RESOURCE AVAILABILITY
  - Lead contact
  - Materials availability
  - Data and code availability
- EXPERIMENTAL MODEL AND SUBJECT DETAILS
  - Cell lines
- METHOD DETAILS
  - Martini coarse-grained simulations
  - Coarse-grained simulations of mutant Kir2.2

- Protein contact network analysis
- Plasmid and mutagenesis
- Transfection and expression evaluation
- Methyl-β-cyclodextrin treatment
- Automated patch clamp recording

- QUANTIFICATION AND STATISTICAL ANALYSIS

SUPPLEMENTAL INFORMATION

Supplemental information can be found online at https://doi.org/10.1016/j.isci.2022.104329.

ACKNOWLEDGMENTS

We thank Ms. Dana Lazarko for her help with performing imaging experiments. We also thank the Imaging Core of Research Resource Center of the UIC for supporting these experiments. This research is supported by NIH NHLBI grants R01HL073965, R01HL141120 R01HL083298, and R01HL122010.

Funding: This research used resources at the Joint Institute for Biological Sciences (JIBS), a DOE Office of Science User Facility operated by the Oak Ridge National Laboratory.

AUTHOR CONTRIBUTIONS

Conceptualization, N.B., S.T.G., B.S.A., and I.L.; Methodology, N.B., S.T.G., S.J.A, A.L.G., B.S.A., and I.L.; Software, N.B., D.K., and B.S.A.; Formal Analysis, N.B. and S.T.G.; Investigation, N.B., S.T.G, C.G.V., and T.V.A.; Resources, A.L.G. and I.L.; Writing – Original Draft, N.B., S.T.G., B.S.A., and I.L.; Writing – Review & Editing, N.B., S.T.G., B.S.A., and I.L.; Visualization, N.B. and S.T.G.; Supervision, A.L.G., B.S.A., and I.L.; Funding Acquisition, A.L.G., B.S.A., and I.L.

DECLARATION OF INTERESTS

The authors declare no competing interests.

Received: December 21, 2021
Revised: March 29, 2022
Accepted: April 26, 2022
Published: May 20, 2022

REFERENCES

Abraham, M.J., Murtola, T., Schulz, R., Páll, S., Smith, J.C., Hess, B., and Lindahl, E. (2015). GROMACS: high performance molecular simulations through multi-level parallelism from laptops to supercomputers. SoftwareX *1–2*, 19–25. https://doi.org/10.1016/j.softx.2015.06.001.

Ahn, S.J., Fancher, I.S., Granados, S.T., Do Couto, N.F., Hwang, C.L., Phillips, S.A., and Levitan, I. (2022). Cholesterol-induced suppression of endothelial Kir channels is a driver of impairment of arteriolar flow-induced vasodilation in humans. Hypertension *79*, 126–138. https://doi.org/10.1161/HYPERTENSIONAHA.121.17672.

Alessandri, R., Souza, P.C.T., Thallmair, S., Melo, M.N., de Vries, A.H., and Marrink, S.J. (2019). Pitfalls of the martini model. J. Chem. Theor. Comput. *15*, 5448–5460. https://doi.org/10.1021/acs.jctc.9b00473.

Baier, C.J., Fantini, J., and Barrantes, F.J. (2011). Disclosure of cholesterol recognition motifs in transmembrane domains of the human nicotinic acetylcholine receptor. Scientific. Rep. *1*, 69. https://doi.org/10.1038/srep00069.

Barbera, N., Ayee, M.A., Akpa, B.S., and Levitan, I. (2018). Molecular dynamics simulations of Kir2.2 interactions with an ensemble of cholesterol molecules. Biophys. J. *115*, 1264–1280. https://doi.org/10.1016/j.bpj.2018.07.041.

Blondel, V.D., Guillaume, J.L., Lambiotte, R., and Lefebvre, E. (2008). Fast Unfolding of Communities in Large Networks" 2008 (10): P10008. J Statist. Mecha. Theory Experim. 1742–5468. https://doi.org/10.1088/1742-5468/2008/10/P10008.

Borcik, C.G., Eason, I.R., Yekefallah, M., Amani, R., Han, R., Vanderloop, B.H., Wylie, B.J., Maryam, Y., Reza, A., Ruixian, H., et al. (2022). A cholesterol dimer stabilizes the inactivated state of an inward-rectifier potassium channel. Angew. Chem. Int. Edition *61*, e202112232. https://doi.org/10.1002/anie.202112232.

Borschel, W.F., Wang, S., Lee, S., and Nichols, C.G. (2017). Control of Kir channel gating by cytoplasmic domain interface interactions. J. Gen. Physiol. *149*, 561–576. https://doi.org/10.1085/jgp.201611719.

Brannigan, G., Hénin, J., Law, R., Eckenhoff, R., and Klein, M.L. (2008). Embedded cholesterol in

the nicotinic acetylcholine receptor. Proc. Natl. Acad. Sci. *105*, 14418–14423. https://doi.org/10.1073/pnas.0803029105.

Bukiya, A.N., Belani, J.D., Rychnovsky, S., and Dopico, A.M. (2011). Specificity of cholesterol and analogs to modulate BK channels points to direct sterol–channel protein interactions. J. Gen. Physiol. *137*, 93–110. https://doi.org/10.1085/jgp.201010519.

Chang, H.M., Reitstetter, R., Mason, R.P., and Gruener, R. (1995). Attenuation of channel kinetics and conductance by cholesterol: an interpretation using structural stress as a unifying concept. J. Membr. Biol. *143*, 51–63. https://doi.org/10.1007/BF00232523.

Clarke, O.B., Caputo, A.T., Hill, A.P., Vandenberg, J.I., Smith, B.J., Gulbis, J.M., Vandenberg, J.I., Smith, B.J., and Gulbis, J.M. (2010). Domain reorientation and rotation of an intracellular assembly regulate conduction in Kir potassium channels. Cell *141*, 1018–1029. https://doi.org/10.1016/j.cell.2010.05.003.

Collins, T.J. (2007). ImageJ for microscopy. BioTechniques *43*, S25–S30. https://doi.org/10.2144/000112517.

Daily, M.D., and Gray, J.J. (2009). Allosteric communication occurs via networks of tertiary and quaternary motions in proteins. PLoS Comput. Biol. *5*, e1000293. https://doi.org/10.1371/journal.pcbi.1000293.

D'Avanzo, N., Hyrc, K., Enkvetchakul, D., Covey, D.F., and Nichols, C.G. (2011). Enantioselective protein-sterol interactions mediate regulation of both prokaryotic and eukaryotic inward rectifier K^+ channels by cholesterol. PLoS One *6*, e19393. https://doi.org/10.1371/journal.pone.0019393.

Di Scala, C., Baier, C.J., Evans, L.S., Williamson, P.T., Fantini, J., and Barrantes, F.J. (2017). Relevance of CARC and CRAC cholesterol-recognition motifs in the nicotinic acetylcholine receptor and other membrane-bound receptors. Curr. Top Membr. *80*, 3–23. https://doi.org/10.1016/bs.ctm.2017.05.001.

Dokholyan, N.V. (2016). Controlling allosteric networks in proteins. Chem. Rev. *116*, 6463–6487. https://doi.org/10.1021/acs.chemrev.5b00544.

Elkins, M.R., Bandara, A., George, A., Pantelopulos, J.E.S., and Hong, M. (2021). Direct observation of cholesterol dimers and tetramers in lipid bilayers. J. Phys. Chem. B. *125*, 1825–1837. https://doi.org/10.1021/acs.jpcb.0c10631.

Epshtein, Y., Chopra, A.P., Rosenhouse-Dantsker, A., Kowalsky, G.B., Logothetis, D.E., and Levitan, I. (2009). Identification of a C-terminus domain critical for the sensitivity of Kir2.1 to cholesterol. PNAS *106*, 8055–8060. https://doi.org/10.1073/pnas.0809847106.

Fantini, J., and Barrantes, F.J. (2013). How cholesterol interacts with membrane proteins: an exploration of cholesterol-binding sites including CRAC, CARC and tilted domains. Front. Physiol. *4*. https://doi.org/10.3389/fphys.2013.00031.

Fürst, O., Nichols, C.G., Lamoureux, G., and D'Avanzo, N. (2014). Identification of a cholesterol-binding pocket in inward rectifier k(+) (Kir) channels. Biophys. J. *107*, 2786–2796. https://doi.org/10.1016/j.bpj.2014.10.066.

Grouleff, J., Sheeba, J.I., Skeby, K.K., and Schiøtt, B. (2015). The influence of cholesterol on membrane protein structure, function, and dynamics studied by molecular dynamics simulations. Biochim. Biophys. Acta (Bba) *1848*, 1783–1795. https://doi.org/10.1016/j.bbamem.2015.03.029.

Gupta, S., Bavro, V.N., D'Mello, R., Tucker, S.J., Vénien-Bryan, C., and Chance, M.R. (2010). Conformational changes during the gating of a potassium channel revealed by structural mass spectrometry. Structure *18*, 839–846. https://doi.org/10.1016/j.str.2010.04.012.

Hedger, G., and Sansom, M.S.P. (2016). Lipid interaction sites on channels, transporters and receptors: recent insights from molecular dynamics simulations. Biochim. Biophys. Acta *1858*, 2390–2400. https://doi.org/10.1016/j.bbamem.2016.02.037.

Henin, J., Salari, R., Murlidaran, S., and Brannigan, G. (2014). A predicted binding site for cholesterol on the GABAA receptor. Biophys. J. *106*, 1938–1949. https://doi.org/10.1016/j.bpj.2014.03.024.

Hibino, H., Inanobe, A., Furutani, K., Murakami, S., Findlay, I., and Kurachi, Y. (2010). Inwardly rectifying potassium channels: their structure, function, and physiological roles. Physiol. Rev. *90*, 291–366. https://doi.org/10.1152/physrev.00021.2009.

Humphrey, W., Dalke, A., and Schulten, K. (1996). VMD: visual molecular dynamics. J. Mol. Graphics *14*, 33–38. https://doi.org/10.1016/0263-7855(96)00018-5.

Ingólfsson, H.I., Melo, M.N., van Eerden, F.J., Arnarez, C., Lopez, C.A., Wassenaar, T.A., Periole, X., de Vries, A.H., Tieleman, D.P., and Marrink, S.J. (2014). Lipid organization of the plasma membrane. J. Am. Chem. Soc. *136*, 14554–14559. https://doi.org/10.1021/ja507832e.

Marrink, S.J., Siewert, and Peter Tieleman, D. (2013). Perspective on the martini model. Chem. Soc. Rev. *42*, 6801–6822. https://doi.org/10.1039/C3CS60093A.

de Jong, D.H., Singh, G., Bennett, W.F.D., Arnarez, C., Wassenaar, T.A., Schäfer, L.V., Periole, X., Tieleman, D.P., and Marrink, S.J. (2013). Improved parameters for the martini coarse-grained protein force field. J. Chem. Theor. Comput. *9*, 687–697. https://doi.org/10.1021/ct300646g.

Kilambi, K.P., and Gray, J.J. (2012). Rapid calculation of protein PKa values using rosetta. Biophys. J. *103*, 587–595. https://doi.org/10.1016/j.bpj.2012.06.044.

Kubo, Y., Adelman, J.P., Clapham, D.E., Jan, L.Y., Karschin, A., Kurachi, Y., Lazdunski, M., Nichols, C.G., Seino, S., and Vandenberg, C.A. (2005). International union of pharmacology. LIV. Nomenclature and molecular relationships of inwardly rectifying potassium channels. Pharmacol. Rev. *57*, 509–526. https://doi.org/10.1124/pr.57.4.11.

Kuenze, G., Vanoye, C.G., Desai, R.R., Adusumilli, S., Brewer, K.R., Woods, H., McDonald, E.F., Sanders, C.R., George, A.L., and Meiler, J. (2020). Allosteric mechanism for KCNE1 modulation of KCNQ1 potassium channel activation. Elife *9*, e57680. https://doi.org/10.7554/elife.57680.

Kumar, G.A., Sarkar, P., Tomasz, M.S., Jafurulla, M., Singh, S.P., Jana, S., and Chattopadhyay, A. (2021). A molecular sensor for cholesterol in the human serotonin1A receptor. Sci. Adv. *7*, eabh2922. https://doi.org/10.1126/sciadv.abh2922.

Lacin, E., Aryal, P., Glaaser, I.W., Bodhinathan, K., Tsai, E., Marsh, N., Tucker, S.J., Mark, S., Sansom, P., and Slesinger, P.A. (2017). Dynamic role of the tether helix in PIP2-dependent gating of a G protein–gated potassium channel. J. Gen. Physiol. *149*, 799–811. https://doi.org/10.1085/jgp.201711801.

Lee, S.J., Ren, F., Eva-Maria, Z.P., Heyman, S., Stary-Weinzinger, A., Yuan, P., Nichols, C.G., and Colin, G. (2016). Structural basis of control of inward rectifier Kir2 channel gating by bulk anionic phospholipids. J. Gen. Physiol. *148*, 227–237. https://doi.org/10.1085/jgp.201611616.

Levitan, I., Fang, Y., Rosenhouse-Dantsker, A., and Romanenko, V. (2010). Cholesterol and ion channels. In Cholesterol Binding and Cholesterol Transport Proteins, *51*, J.R. Harris, ed (Springer Science), pp. 509–549. Subcellular Biochemistry.

Levitan, I., Singh, D.K., and Rosenhouse-Dantsker, A. (2014). Cholesterol binding to ion channels. Front. Physiol. *5*. https://doi.org/10.3389/fphys.2014.00065.

Lundbæk, J.A., Birn, P., Girshman, J., and Andersen, O.S. (1996). Membrane stiffness and channel function. Biochemistry *35*, 3825–3830. https://doi.org/10.1021/bi952250b.

Lyskov, S., Chou, F.C., Conchúir, S.Ó., Der, B.S., Drew, K., Kuroda, D., Xu, J., Weitzner, B.D., Renfrew, P.D., Sripakdeevong, P., et al. (2013). Serverification of molecular modeling applications: the rosetta online server that includes everyone (ROSIE). PLoS. One. *8*, e63906. https://doi.org/10.1371/journal.pone.0063906.

Mathiharan, Y.K., Glaaser, I.W., Zhao, Y., Robertson, M.J., Skiniotis, G., and Slesinger, P.A. (2021). Structural insights into GIRK2 channel modulation by cholesterol and PIP2. Cell. Rep. *36*, 109619. https://doi.org/10.1016/j.celrep.2021.109619.

van Meer, G., Voelker, D.R., and Feigenson, G.W. (2008). Membrane lipids: where they are and how they behave. Nat. Rev. Mol. Cell. Biol. *9*, 112–124. https://doi.org/10.1038/nrm2330.

Melo, M.N., Ingólfsson, H.I., and Marrink, S.J. (2015). Parameters for martini sterols and hopanoids based on a virtual-site description. J. Chem. Phys. *143*, 243152. https://doi.org/10.1063/1.4937783.

Pegan, S., Arrabit, C., Zhou, W., Kwiatkowski, W., Collins, A., Slesinger, P.A., and Choe, S. (2005). Cytoplasmic domain structures of Kir2.1 and Kir3.1 show sites for modulating gating and rectification. Nat. Neurosci. *8*, 279–287. https://doi.org/10.1038/nn1411.

Picazo-Juarez, Giovanni, S.R., Nieto-Posadas, A., Llorente, I., Jara-Oseguera, A., Briggs, M., McIntosh, T.J., Simon, S.A., Ladron-de-Guevara, E., Islas, L.D., and Rosenbaum, T. (2011). Identification of a binding motif in the S5 helix that confers cholesterol sensitivity to the TRPV1 ion channel. J. Biol. Chem. *286*, 24966–24976. https://doi.org/10.1074/jbc.M111.237537.

Romanenko, V.G., Fang, Y., Byfield, F., Travis, A.J., Vandenberg, C.A., Rothblat, G.H., and Levitan, I. (2004). Cholesterol sensitivity and lipid raft targeting of Kir2.1 channels. Biophys. J. *87*, 3850–3861. https://doi.org/10.1529/biophysj.104.043273.

Romanenko, V.G., Rothblat, G.H., and Levitan, I. (2002). Modulation of endothelial inward rectifier K+ current by optical isomers of cholesterol. Biophys. J. *83*, 3211–3222. https://doi.org/10.1016/s0006-3495(02)75323-x.

Rosenhouse-Dantsker, A. (2017). Insights into the molecular requirements for cholesterol binding to ion channels. Curr. Top Membr. *80*, 187–208. https://doi.org/10.1016/bs.ctm.2017.05.003.

Rosenhouse-Dantsker, A., and Levitan, I. (2012). Insights into structural determinants of cholesterol sensitivity of Kir channels. In Cholesterol Regulation of Ion Channels and Receptors, *47–67*, I. Levitan, ed (Hoboken, New Jersey: Wiley-Blackwell).

Rosenhouse-Dantsker, A., Epshtein, Y., and Levitan, I. (2014). Interplay between lipid modulators of Kir2 channels: cholesterol and PIP2. Comput. Struct. Biotechnol. J. *11*, 131–137. https://doi.org/10.1016/j.csbj.2014.09.007.

Rosenhouse-Dantsker, A., Logothetis, D.E., and Levitan, I. (2011). Cholesterol sensitivity of KIR2.1 is controlled by a belt of residues around the cytosolic pore. Biophys. J. *100*, 381–389. https://doi.org/10.1016/j.bpj.2010.11.086.

Rosenhouse-Dantsker, A., Noskov, S., Durdagi, S., Logothetis, D.E., and Levitan, I. (2013). Identification of novel cholesterol-binding regions in Kir2 channels. J. Biol. Chem. *288*, 31154–31164. https://doi.org/10.1074/jbc.M113.496117.

Sillitoe, I., Lewis, T.E., Cuff, A., Das, S., Ashford, P., Dawson, N.L., Furnham, N., Laskowski, R.A., Lee, D., Lees, J.G., et al. (2015). CATH: comprehensive structural and functional annotations for genome sequences. Nucleic. Acids. Res. *43*, D376–D381. https://doi.org/10.1093/nar/gku947.

Singh, A.K., McMillan, J., Bukiya, A.N., Burton, B., Parrill, A.L., and Dopico, A.M. (2012). Multiple cholesterol recognition/interaction amino acid consensus (CRAC) motifs in cytosolic C tail of Slo1 subunit determine cholesterol sensitivity of Ca2+- and voltage-gated K+ (BK) channels. J. Biol. Chem. *287*, 20509–20521. https://doi.org/10.1074/jbc.M112.356261.

Singh, D.K., Rosenhouse-Dantsker, A., Nichols, C.G., Enkvetchakul, D., and Levitan, I. (2009). Direct regulation of prokaryotic Kir channel by cholesterol. J. Biol. Chem. *284*, 30727–30736. https://doi.org/10.1074/jbc.M109.011221.

Singh, D.K., Tzu-Pin, S., Enkvetchakul, D., and Levitan, I. (2011). Cholesterol regulates prokaryotic Kir channel by direct binding to channel protein. Biochim. Biophys. Acta *1808*, 2527–2533. https://doi.org/10.1016/j.bbamem.2011.07.006.

Siuda, I., and Thøgersen, L. (2013). Conformational flexibility of the leucine binding protein examined by protein domain coarse-grained molecular dynamics. J. Mol. Model. *19*, 4931–4945. https://doi.org/10.1007/s00894-013-1991-9.

Vanoye, C.G., Reshma, R.D., Fabre, K.L., Gallagher, S.L., Potet, F., DeKeyser, J.M., Macaya, D., Meiler, J., Sanders, C.R., George, A.L., Jr., et al. (2018). High-throughput functional evaluation of KCNQ1 decrypts variants of unknown significance. Circ. Genomic Precision Med. *11*, e002345. https://doi.org/10.1161/circgen.118.002345.

Vanoye, C.G., and Reuss, L. (1999). Stretch-activated single K+ channels account for whole-cell currents elicited by swelling. Proc. Natl. Acad. Sci. *96*, 6511–6516. https://doi.org/10.1073/pnas.96.11.6511.

Wang, S., Vafabakhsh, R., Borschel, W.F., Ha, T., and Nichols, C.G. (2016). Structural dynamics of potassium-channel gating revealed by single-molecule FRET. Nat. Struct. Mol. Biol. *23*, 31–36. https://doi.org/10.1038/nsmb.3138.

Wassenaar, T.A., Ingólfsson, H.I., Böckmann, R.A., Tieleman, D.P., and Marrink, S.J. (2015). Computational lipidomics with insane: a versatile tool for generating custom membranes for molecular simulations. J. Chem. Theor. Comput. *11*, 2144–2155. https://doi.org/10.1021/acs.jctc.5b00209.

Webb, B., and Sali, A. (2017). Protein structure modeling with MODELLER functional genomics: methods and protocols, edited by michael kaufmann, claudia klinger, and andreas savelsbergh. Methods Mol. Biol. 39–54. https://doi.org/10.1007/978-1-4939-7231-9_4.

Yao, X.Q., Momin, M., and Hamelberg, D. (2018). Elucidating allosteric communications in proteins with difference contact network analysis. J. Chem. Inf. Model *58*, 1325–1330. https://doi.org/10.1021/acs.jcim.8b00250.

Zakany, F., Kovacs, T., Panyi, G., and Varga, Z. (2020). Direct and indirect cholesterol effects on membrane proteins with special focus on potassium channels. Biochim. Biophys. Acta (Bba) - Mol. Cell Biol. Lipids *1865*, 158706. https://doi.org/10.1016/j.bbalip.2020.158706.

Zidovetzki, R., and Levitan, I. (2007). Use of cyclodextrins to manipulate plasma membrane cholesterol content: evidence, misconceptions and control strategies. Biochim. Biophys. Acta (Bba) - Biomembranes *1768*, 1311–1324. https://doi.org/10.1016/j.bbamem.2007.03.026.

STAR★METHODS

KEY RESOURCES TABLE

REAGENT or RESOURCE	SOURCE	IDENTIFIER
Bacterial and virus strains		
pCMV6-AC-GFP vector- NM_021012	Origene	RG207051
Chemicals, peptides, and recombinant proteins		
Dulbecco's Modified Eagle F-12	GIBCO/Invitrogen,	11330032
Penicillin/Streptomycin	Sigma Aldrich	P4333
Methyl-β-cyclodextrin	Sigma Aldrich	C4767
Wheat Germ Agglutinin Stain	Biotium	CF555
Electroporation Buffer	MaxCyte Inc.	EBR100
Critical commercial assays		
QuikChange	Agilent	200518
Nucleobond Xtra Maxi EF	Macherey-Nagel Inc	740424.50
Maxcyte STX system	MaxCyte Inc	SOC-1x2
Experimental models: Cell lines		
Hamster: CHO-K1 cells	ATCC	CRL 9618
Software and algorithms		
Gromacs 5.1	(Abraham et al., 2015)	http://www.gromacs.org
Martini force field	(de Jong et al., 2013)	http://cgmartini.nl
VMD 1.9.2	(Humphrey et al. 1996)	https://www.ks.uiuc.edu/Research/vmd/
martinize.py	(de Jong et al., 2013)	https://github.com/cgmartini/martinize.py
insane.py	(Wassenaar et al., 2015)	http://www.cgmartini.nl/images/tools/insane/insane.py
ImageJ	(Collins 2007)	(https://imagej.nih.gov/ij/

RESOURCE AVAILABILITY

Lead contact

Further information and request for reagents may be directed to, and will be fulfilled by the lead authors, Irena Levitan (levitan@uic.edu).

Materials availability

This study did not generate any novel reagents and all materials used in this study are reported either the main text or in the supplemental information.

Data and code availability

- All data reported in this paper will be shared by the lead contact upon request.
- This paper does not report original code.
- Any additional information required to reanalyze the data reported in this paper is available from the lead contact upon request.

EXPERIMENTAL MODEL AND SUBJECT DETAILS

Cell lines

Chinese hamster ovary cells (CHO-K1; CRL 9618, American Type Culture Collection, Manassas VA, USA) were grown in Dulbecco's Modified Eagle's F-12 nutrient mixture medium (GIBCO/Invitrogen, San Diego,

CA, USA) supplemented with 10% fetal bovine serum (FBS) and an antibiotic mix of penicillin (50 units·ml−1), streptomycin (50 μg·ml−1) (Sigma Aldrich, St. Louis, MO, USA), at 37°C in 5% CO2.

METHOD DETAILS

Martini coarse-grained simulations

Crystal structures for two states of the Kir2.2 channel, the open (PDB ID: 3SPI) and closed (PDB ID: 3JYC) states, were obtained from the RCSB protein data bank. Both the open and closed states of the Kir2.2 channel were crystallized from *gallus gallus*-derived protein, which shares 90% homology with human Kir2.2. In both crystal structures, missing residues were modeled with the Modeller9.16 program (Webb and Sali 2017). Atomistic protein structures were converted to a Martini coarse-grained topology using the martinize.py script, downloaded from the Martini website (http://cgmartini.nl/index.php/tools2/proteins-and-bilayers/204-martinize). A domain-specific version of the ElNeDyn elastic network was also used, wherein the cytosolic and transmembrane domains of the channel were parameterized with separate elastic networks (Barbera et al., 2018; Siuda and Thøgersen 2013). The residues comprising each domain were determined by the CATH database (Sillitoe et al., 2015). The transmembrane domain consisted of residues 60 to 190, with the remaining residues making up the cytosolic domain. Elastic networks were defined for each subunit separately. To determine amino acid protonation states and charges, pKa calculations were ran using Rosetta via the ROSIE server (Kilambi and Gray 2012; Lyskov et al., 2013). Calculated pKa values are listed in Table S1.

Two different POPC model membrane systems were constructed using the insane.py script (http://cgmartini.nl/index.php/tools2/proteins-and-bilayers). These membranes differed only in their cholesterol content of 30 mol% or 15 mol% – representing, respectively, a typical mol% of cholesterol in the plasma membranes of mammalian cells (van Meer et al., 2008; Ingólfsson et al., 2014) and the experimental conditions in cholesterol-depleted cells (Zidovetzki and Levitan 2007). The bilayer was constructed such that cholesterol was randomly distributed in the xy plane, subject to a zone of exclusion extending radially 75 Angstroms beyond the Kir channel. For cholesterol, we used the coarse-grained parameterization involving virtual sites, described in Melo et al. (Melo et al. 2015). Simulations were run using the GROMACS simulation package version 5.0.7(Abraham et al., 2015) with the MARTINI 2.2 force field (de Jong et al., 2013).

Simulations were run with a 3-step equilibration followed by a 20 μs NPT simulation: first, position restraints were applied to Kir2.2 in the initial 100 ns equilibration step, replaced by a flat-bottom restraint in the second equilibration step. A flat-bottom position restraint was applied to membrane cholesterol in steps 1 and 2 to prevent sterol-protein interaction prior to protein and membrane equilibration. In the final step, all restraints were removed. The Berendsen pressure coupling algorithm was replaced with a Parrinello-Rahman coupling algorithm during the subsequent 20 μs NPT production run. Snapshots were taken every 200 ps. This simulation protocol was repeated 4 times, in each case with re-initialized velocities.

Coarse-grained simulations of mutant Kir2.2

For the *in silico* mutations of the channel, the Modeller9.16 program (Webb and Sali 2017) was used to swap either Histidine 222 or Valine 265 on the closed state of the channel (PDB ID: 3JYC). Simulation systems were constructed as above, with either 15 mol% or 30 mol% cholesterol. Simulations with the mutant channel were equilibrated as above, and run for 5 microseconds. For each mutant channel system, the simulation protocol was repeated 5 times.

Protein contact network analysis

A protein contact network of the Kir2.2 channel was generated for each conformational state (open and closed) and at each membrane cholesterol concentration (15 and 30 mol%). The procedure to generate these networks was adopted from the work of Yao et al. (Yao et al. 2018). For each pair of residues in the channel, a contact probability was calculated as follows:

$$p_{ij}^{\alpha} = \frac{n_{contact,ij}}{N}\Big|_{\alpha} \qquad \text{(Equation 1)}$$

where $n_{contact}$ is the number of simulation frames in which a pair of residues *i* and *j* were within a 6 Å cutoff distance, N is the total simulation length, and α is the simulation condition. A protein contact network for a given condition was constructed from all pairwise residue interactions that persisted for greater than 90%

of that simulation condition. Because Kir2.2 is a tetramer composed of 4 identical subunits, we treated the same residue on each subunit separately when calculating its pairwise contact probabilities and generated an average of the results. Likewise, for residues at a subunit interface we calculated contact probabilities for residue-residue interactions across subunits in addition to interactions within subunits. To create a binary representation of dynamically conserved residue-residue contacts, we then generated a consensus network (C_{ij}). The consensus network was defined by those residue-residue interactions that persisted for at least 90% of the simulation time in all four simulation conditions:

$$C_{ij} = \begin{cases} 1 \; if \; p_{ij}^{\alpha} > 0.9 \; \forall \; \alpha \\ 0 \; otherwise \end{cases} \quad \text{(Equation 2)}$$

By applying a Louvain clustering algorithm (Blondel et al., 2008) to this network, we partitioned the dynamically conserved contacts into separate modularity groups that can be interpreted as domains of coherent motion. We then assessed the effect of cholesterol on interactions both between and within domains. To calculate the change in contact between two domains, a domain difference contact network (DDCN) was generated using the following formula:

$$DDCN_{XY} = \sum_{i \in X} \sum_{j \in Y} \left(p_{ij}^{\alpha} - p_{ij}^{\beta} \right) \quad \text{(Equation 3)}$$

where pij is the pairwise contact probability of residues i and j, with i drawn from domain (i.e., modularity group) X and j drawn from domain Y, and the difference is calculated between simulation conditions α and β. The change in residue contacts within a single domain, was calculated as:

$$DDCN_{XX} = \sum_{i \in X} \sum_{j \in X} \left(p_{ij}^{\alpha} - p_{ij}^{\beta} \right) \quad \text{(Equation 4)}$$

Plasmid and mutagenesis

Full-length cDNA encoding wild-type (WT) or mutant human potassium inwardly rectifying channel 2.2 (KCNJ12, NM_021012) (Origene, Cat #: RG207051, Rockville, MD, USA) was engineered in the vector pCMV6-AC-GFP vector. KCNJ12 mutants were introduced using QuikChange (Agilent technologies, Santa Clara, CA, USA) with primers designed using the online QuikChange primer design tool, (http://www.genomics.agilent.com/primerDesignProgram.jsp). Plasmid DNAs were sequenced and the clones with confirmed mutation were amplified using an endotoxin-free plasmid extraction method (Nucleobond Xtra Maxi EF, Macherey-Nagel Inc., Bethlehem, PA, USA) and re-suspended in endotoxin-free water.

Transfection and expression evaluation

Plasmids encoding WT or mutant KCNJ12 were transiently transfected into CHO-K1 cells by electroporation using the Maxcyte STX system (MaxCyte Inc., Gaithersburg, MD, USA). CHO cells grown to 70-80% confluency were harvested using 0.25% trypsin. An aliquot of cell suspension was used to determine cell number and viability on an automated cell counter (ViCell, Beckman Coulter, Brea, CA, USA). Remaining cells were collected by gentle centrifugation (160 × g, 4 minutes), washed with 5 ml electroporation buffer (EBR100, MaxCyte Inc.), and re-suspended in electroporation buffer at a density of 10^8 viable cells/ml. Each electroporation was performed using 100 µl of cell suspension and 4ug of plasmid. Cells were gently re-suspended in culture media and transferred to a T75 tissue culture flask and grown for 48 hrs at 37°C in 5% CO_2. After this period, cells were harvested, counted, transfection efficiency determined by flow cytometry (see below), and then frozen in 1 ml aliquots at 1.5×10^6 viable cells/ml in liquid N_2 until used in experiments (Vanoye et al., 2018; Kuenze et al., 2020). Transfection efficiency of Kir 2.2-GFP wild-type and mutant channels was evaluated by flow cytometry (CytoFLEX, Beckman Coulter) using a 488 nm laser. Forward scatter (FSC) and side scatter (SSC) were used to gate single viable cells and to eliminate doublets, dead cells and debris. The percentage (%) and the mean fluorescence intensity (MFI) of green fluorescent (FITC) cells was determined from the gated cell population. The analyses were made using FlowJo® (Tree Star, Inc.). Additionally, membrane expression was evaluated with confocal microscopy in a Zeiss LSM 710 Confocal Microscope, with a 408-30 nm, 488 nm-argon, and 561 nm-DPSS 561-10 laser diode lines and 63X water immersion objective. To define the cell membrane, Wheat Germ Agglutinin, CF555 (Biotium) stain was used, following the manufacturer's instruction. Images were analyzed using ImageJ software (https://imagej.nih.gov/ij/ freely available from National Institutes of Health).

Methyl-β-cyclodextrin treatment

Transfected cells were thawed the day before the experiment, grown for ~10 hours at 37°C in 5% CO2, and then grown overnight at 28°C in 5% CO_2 to increase channel expression at the plasma membrane. On the day of the experiments, fresh 2.5mM Methyl-β-cyclodextrin (MBCD) was prepared on F-12 media without FBS. Cells were incubated for 45 min at 37ºC in the MBCD media to allow the removal of membrane cholesterol.

Automated patch clamp recording

Prior to the experiment, cells were suspended using 0.25% trypsin in cell culture media. Cells were then diluted to 200,000 cells/ml with electrophysiology external solution, while shaking on a rotating platform at 200 rpm to recover 40 minutes at 15°C. Automated patch clamp recording was performed using the Syncropatch 768 PE platform (Nanion Technologies, Munich, Germany) and 384-well, single-hole recording chips with medium resistance (2-4 MΩ). The recording electrophysiology external solution contained (in mM): KCl 140, $CaCl_2$ 2, $MgCl_2$ 1, HEPES 10, glucose 5, with the final pH adjusted to 7.4 with NaOH. The internal solution contained (in mM): KF 60, KCl 50, NaCl 10, HEPES 10, EGTA 10, 2 MgATP, with the final pH adjusted to 7.2 with KOH, all chemicals were obtained from Sigma-Aldrich (St. Louis, MO, USA).

Pulse generation and data collection were carried out with PatchController384 V.1.3.0 and DataController384 V1.2.1 software (Nanion Technologies). Whole-cell currents were filtered at 3 kHz and acquired at 10 kHz. Whole-cell currents were recorded at room temperature in the whole-cell configuration from −120 to +60 mV (in 20 mV steps) 10 and 495 ms after the start of the voltage pulse from a holding potential of 0 mV. Whole-cell currents were not leak-subtracted. The contribution of background currents was determined by recording before and after addition of 5 mM $BaCl_2$. The currents recorded in the presence of $BaCl_2$ were digitally subtracted from recordings done in the absence of $BaCl_2$. Only $BaCl_2$-sensitive currents recorded from cells with seal resistance $\geq$0.1 GΩ, series resistance $\leq$20 MΩ and capacitance $\geq$1 pF were used for analysis.

QUANTIFICATION AND STATISTICAL ANALYSIS

Data was analyzed with a one-way ANOVA ($p < 0.05$) using GraphPad Prism 6. Patch data were analyzed and plotted using a combination of DataController384 V1.2.1 (Nanion Technologies) and Excel (Microsoft Office 365, Microsoft) were used for analysis of current density. Whole-cell currents were normalized for membrane capacitance and results expressed as mean $\pm$ SEM. The number of cells used for each experimental condition is shown in the figure legends. The threshold for statistical significance was $p \leq 0.05$.